出國報告（出國類別：開會）

參加「第 17 屆世界沉積大會 -17th International Sedimentological Congress」出國報告

服務機關：中國石油股份有限公司
姓名職稱：吳榮章　微古生物科學師
派赴國家：日本福岡
出國期間：95.8.28—95.9.3
報告日期：95.10.27

摘 要

多年來本所未派員參與有關國際沉積研討會，然而從事盆地分析研究並協助現場單位探勘為本所之重點工作，在有關盆地地層架構、地層層序與對比、沉積環境分析、沉積相研究等課題是盆地探勘及石油系統的基礎，亦為礦區評估之首要工作。而對於目前公司探勘策略方向要走向國外，故本次奉派參與第十七屆世界沉積大會，研討有關各種層序地層、沉積相、古環境等及其在油氣探勘之應用，並收集國際層序地層分析與研究論文及相關資料，並為國外探勘作業奠定礦區評估層序地層基礎分析架構。

具有成果有：

1. 可運用生物地層、沉積環境分析、沉積相及層序分析建立地層架構，做為盆地分析之基礎。
2. 收集新近國際地層對比資料建立研究礦區之對比。
3. 進行相關技術之交流。
4. 日後可應用於國內外礦區評估及探勘作業。

目 錄

參加國際層序地層及油氣封閉探勘相關研討會
-17thInternational Sedimentological Congress 出國報告

壹、出國目的

本次出國參與第17屆世界沉積大會(17thInternational Sedimentological Congress)與本年度及石油基金計畫「台灣西北部竹苗區層序地層架構與油氣封閉分析」項下完全契合。

其主要目的研討有關各種層序地層、沉積相、古環境等及其在油氣探勘之應用,收集國際層序地層分析與研究論文及相關資料實為當務之急,並為國外探勘作業奠定礦區評估層序地層基礎分析架構。

貳、出國行程

職於95年8月28日從桃園中正機場出發，前往日本福岡參加第17屆世界沉積大會,於95年9月3日返國,共計7日，其主要行程及工作內容如下：

日 期	地　　點	工　作　內　容
95/08/28	桃園中正機場 →福岡	啟程
95/08/29-09/02	福岡	參與17屆世界沉積大會(17^{th}International Sedimentological Congress)研討
95/09/03	福岡 →桃園中正機場	返程

參、參與第 17 屆世界沉積大會

一、緣起：

從事盆地分析研究並協助現場單位探勘為本所之重點工作，在有關盆地地層架構、地層層序與對比、沉積環境分析、沉積相研究等課題是盆地探勘及石油系統的基礎，亦為礦區評估之首要工作。而多年來本所未派員參與有關國際沉積研討會，而對於探勘策略方向要走向國外，故派員研討有關各種層序地層、沉積相、古環境等及其在油氣探勘之應用，並收集國際層序地層分析與研究論文及相關資料實為當務之急，並為國外探勘作業奠定礦區評估層序地層基礎分析架構。

二、 目標：

本公司為掌握自產能源，以支援國家經濟建設之發展，歷年來積極在本省陸海域從事油氣探勘，而其油氣探勘大都集中在中新統及其以後之地層為主，且主要之構造幾已探勘殆盡，目前油氣測勘作業益形艱難，再加上國外探勘景氣已見回春，故為加強突破目前探勘瓶頸，致力尋求本公司陸海域盆地油氣探勘之第二春，有必要結合地球物理、地球化學及石油地質多領域之等專業技術，進而整合評估與研究，期以探討探勘地區之油氣封閉。尤其是高解析之層序地層分析及對比應用於石油系統及油氣封閉之探勘尤為重要。其核心技術亦有待加強突破！

三、 實施要領：

地層封閉的研究其最基本需正確建立其地層架構及對比，而層序地層分析及對比則為最基礎及必備之應用工具之一，亦為震測剖面解釋之主要架構控制之一。

另外從過去之油氣探勘經驗得知，台灣陸海域地區仍有相當的油氣潛能。然此一地區之沉積環境因陸相、濱海、陸棚；至西南部具陸棚和陸坡交界，整體沉積環境變化快速，且加上後期蓬萊造山運動影響，構造形貌亦相當複雜。為求突破探勘瓶頸，有效評估油氣封閉潛能，亟需加強精細之地層層序分析，故派員與國際盛名之世界沉積大會，收集相關資訊，並進行該技術交流，吸取寶貴經驗，以應用於國內外礦區評估及探勘作業上。

四、成果：

1. 可運用生物地層、沉積環境分析、沉積相及層序分析建立地層架構，做為盆地分析之基礎。
2. 收集新近國際地層對比資料建立研究礦區之對比。
3. 進行相關技術之交流。
4. 日後可應用於國內外礦區評估及探勘作業。

第 17 屆世界沉積大會今年於日本福岡舉行，見圖一，參與大會專業人士超過兩千多人，會中分別有各項專題及會場舉行，並有各種相關專業論文及壁報論文發表，亦有各種野外勘查及專業訓練課程（可惜因時間限制大皆未能參與），是目前世界上有關沉積研究最大亦最高之國際研討會，參見圖二～圖八及照片一～照片十二。

有關大會Special Symposia 之論文主題及會場如下：

Theme 1:Tectonics, climate, and sedimentation

SS1-1 Sedimentation in and around magmatic arcs in relation to tectonics and volcanism

Conveners: C. Busby (UCSB) and K. Kiminami (Yamaguchi Univ.)

SS1-2 Monsoons and the Himalaya: tectonics-climate and land-ocean linkages

Conveners: P. Clift (Univ. Aberdeen), H. Zheng (Tongji Univ.) and R. Tada (Univ. Tokyo)

SS1-3 Continental margin sedimentation and deep-water sedimentary systems

Conveners: O. Martinsen (Norsk) and K. Hoyanagi (Shinshu Univ.)

Theme 2: Environmental sedimentology and human society

SS2-1 Coastal environments and human activity

Conveners: S. Goodbred (Vanderbilt Univ.), S. Chun (Chonnam Nat. Univ.), A. Bartholomae (Senckenberg Inst.) and Y. Saito (GSJ/AIST)

SS2-2 Catastrophic sedimentary processes: mechanisms and hazard mitigation

Conveners: F. Nanayama (GSJ/AIST), K. Ikehara (GSJ/AIST) and S. Kiyokawa (Kyushu Univ.)

Theme 3:New targets and innovation in resource sedimentology

SS3-1 Gas hydrates: origin, exploration and resource potential

Conveners: T. Collett (USGS), C. Paull (MBARI) and R. Matsumoto (Univ. Tokyo)

SS3-2 3D seismic technology for exploration and sediment body analysis

Conveners: H. Posamentier (Anadarko) and O. Takano (JAPEX)

Theme 4: Evolution of the biosphere and geosphere

SS4-1 Microbial processes and products in sedimentary systems

Conveners: J. McKenzie (ETH) and A. Kano (Hiroshima Univ.

SS4-2 Boundary events and global change

Conveners: M. Tucker (Univ. Durham) and Y. Kakuwa (Univ. Tokyo)

Theme 5: Frontiers in sedimentology

SS5-1 Role of sedimentology in Earth drilling projects

Conveners: A. Taira (JAMSTEC), H. Kudrass (BGR), P. Delany (UCSC), A. Mix (Oregon St. Univ.), W. Soh (JAMSTEC) and N. Suzuki (Hokkaido Univ.)

SS5-2 Extraterrestrial sedimentology

Conveners: H. Miyamoto (Univ. Tokyo) and G. Ori (Univ. G. d'Annunzio)

SS5-3Integrated strata analysis

Conveners: C. Nittrouer (Univ. Washington), S. Berne (IFREMER), J. Syvitski (INSTAAR) and Y. Saito (GSJ/AIST)

Technical Sessions

All participants are invited to submit abstracts for oral and poster presentations.

Theme 1: Siliciclastic depositional systems and sequence stratigraphy

Conveners:D. Nummedal (CSM), A. Schaefer (Univ. Bonn), A. T-S Lin (Nat. Central Univ.),
T. Sakai (Shimane Univ.) and K. Hoyanagi (Shinshu Univ.)

TS1-1 Glacial depositional systems

TS1-2 Aeolian systems

TS1-3 Lacustrine and fluvial systems

TS1-4 Barrier island and estuarine systems

TS1-5 Delta and fan delta systems

TS1-6 Shelf and shallow marine systems

TS1-7 Resedimentation and deep-water sedimentary systems

TS1-8 Sea-level changes and sequence architectures

Theme 2: Carbonates and evaporites

Conveners:W. Piller (Graz Univ.), G. Cabioch (IRD), D. Chen (Chinese Acad. Sci.), H. Matsuda (Kumamoto Univ.) and Y. Iryu (Tohoku Univ.)

TS2-1 Carbonate sediments: environments and processes

TS2-2 Carbonate diagenesis, geochemistry and hydrogeochemistry

TS2-3 Daily to decadal environmental records in skeletal carbonates

TS2-4 Dolomite and dolomitization

TS2-5 Depositional processes and climatic records of freshwater carbonates

TS2-6 Microbialites

TS2-7 Evaporites

Theme 3: Sedimentary processes: experiments, simulations and field observations

Conveners:J. Southard (MIT), G. Parker (Univ. Illinois), Y.

Miyata (Yamaguchi Univ.), T. Muto (Nagasaki Univ.) and M. Yokokawa (Osaka Inst. Tech.)

TS3-1 Physical processes of sedimentary structures

TS3-2 Shallow-marine processes and sedimentation

TS3-3 Density flow processes and sedimentation

TS3-4 Experimental stratigraphy

Theme 4: Basin analysis and numerical modeling

Conveners:C. Busby (UCSB), C. Paola (Univ. Minnesota) and O. Takano (JAPEX)

TS4-1 Tectonics and sedimentation

TS4-2 Sedimentation in rift basins

TS4-3 Sedimentation in strike-slip and forearc basins

TS4-4 Basin analysis and stratigraphic modelling

Theme 5: Petrology, mineralogy and geochemistry of sediments

Conveners:S. Critelli (Univ. Calabria), H. Yoon (Korea Polar Res. Inst.), M. Kametaka (GSJ/AIST) and K. Yoshida (Shinshu Univ.)

TS5-1 Sandstone petrology: provenance and diagenesis

TS5-2 Clay mineralogy and geochemistry

TS5-3 Siliceous and phosphatic sediments

TS5-4 Ironstone and metalliferous sediments

TS5-5 Inorganic geochemistry and chemostratigraphy

Theme 6: Volcano-sedimentology

Conveners:J. White (Univ. Otago), U. Martin (Würzburg Univ.), K. Nemeth (Massey Univ.) and K. Kano (GSJ/AIST)

TS6-1 Eruptions and tephra dispersal on land and under the sea

TS6-2 Sector collapse, avalanches and lahars

TS6-3 Calderas and volcaniclastic sediments

TS6-4 Facies models in volcanic settings: volcanoes and hydrothermal systems

Theme 7: Marine geology and sedimentology

Conveners:K. Ikehara (GSJ/AIST) , M. Li (BIO/GSC) and K. Arai (GSJ/AIST)

TS7-1 Marine sediments and sedimentology

TS7-2 Sediments and sedimentary processes on continental shelves

TS7-3 Particle transport processes in the marine environment; from suspended/sinking particle to sediment

TS7-4 Cold seeps, gas hydrates and related phenomena: past and modern

Theme 8: Palaeontology and sedimentology *Conveners:G. Pemberton (Univ. Alberta), H. Ando (Ibaraki Univ.) and Y. Kondo (Kochi Univ.)*

TS8-1 Fossil records in stratigraphic framework

TS8-2 Ichnology and sedimentary facies

TS8-3 Palaeoecology, taphonomy and sedimentary records

TS8-4 Microfossil and organic records for sedimentary environment analyses

Theme 9: Environmental and applied sedimentology

Conveners:K. Kashima (Kyushu Univ.), F. Nanayama (GSJ/AIST) and T. Ueki (GSJ/AIST)

TS9-1 Environmental sedimentology

TS9-2 Holocene stratigraphy and sedimentation

TS9-3 Tsunami, storm hazards and related sediments

TS9-4 Landslides, liquefaction and gravity flow

TS9-5 Flood hazards and related sediments

Theme 10: Resource sedimentology

Conveners:H. Arato (Teikoku Oil Co.), A. Mizobe (Teikoku Oil Co.), T. Nakanishi (INPEX) and O. Takano (JAPEX)

TS10-1 Hydrocarbon deposits; coal, petroleum and gas

TS10-2 Organic sedimentology and geochemistry

TS10-3 Placer deposits and aggregate resources

Theme 11: Palaeoclimate and sedimentation

Conveners:Y. Il Lee (Seoul Nat. Univ.), S. Ji (NIGLAS), L. Jansa (BIO/GSC), T. Sakai (Kyushu Univ.) and H. Fukusawa (Tokyo Met. Univ.)

TS11-1 Lake sediment information and environmental change

TS11-2 Sedimentary record of deep marine Cretaceous: an archive of palaeoceanography, palaeoclimate and global tectonics

TS11-3 Palaeoclimate of the Cretaceous in Asia

TS11-4 Palaeoclimate of the Cenozoic Asia

TS11-5 Sediment record on palaeoceanography and palaeoclimatology

Theme 12: Sedimentology: past, present and future

Conveners:G.M. Friedman (formerly President, IAS), H. Okada (formerly President, SSJ),H. Machiyama (JAMSTEC), O. Takano (JAPEX) and K. Hoyanagi (Shinshu Univ.)

TS12-1 History of sedimentology

TS12-2 New technology for sediment analysis

TS12-3 IODP and ICDP: new horizon of sedimentology

TS12-4 Extraterrestrial Sedimentology: techniques and interpretations

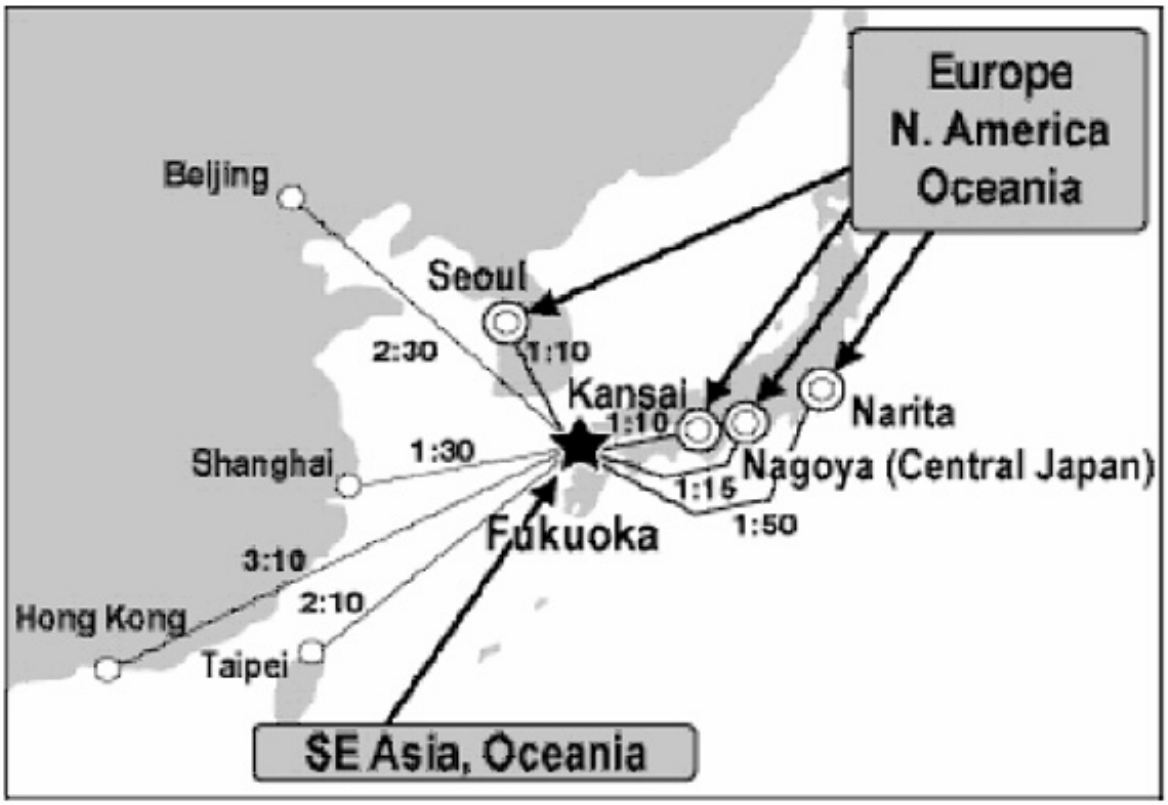

圖一、第 17 屆世界沉積大會 2006 於日本福岡舉行

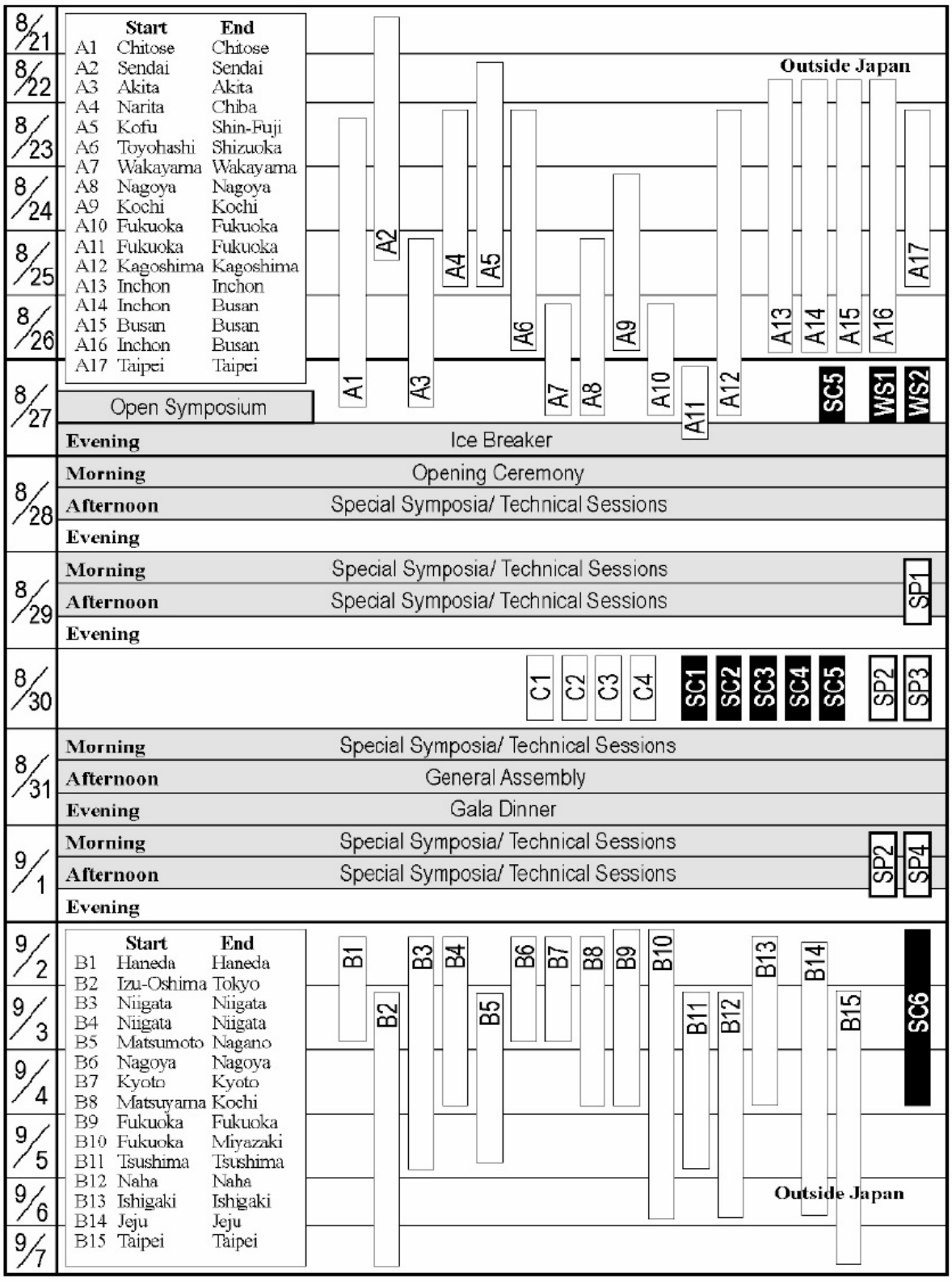

圖二、第 17 屆沉積大會時程

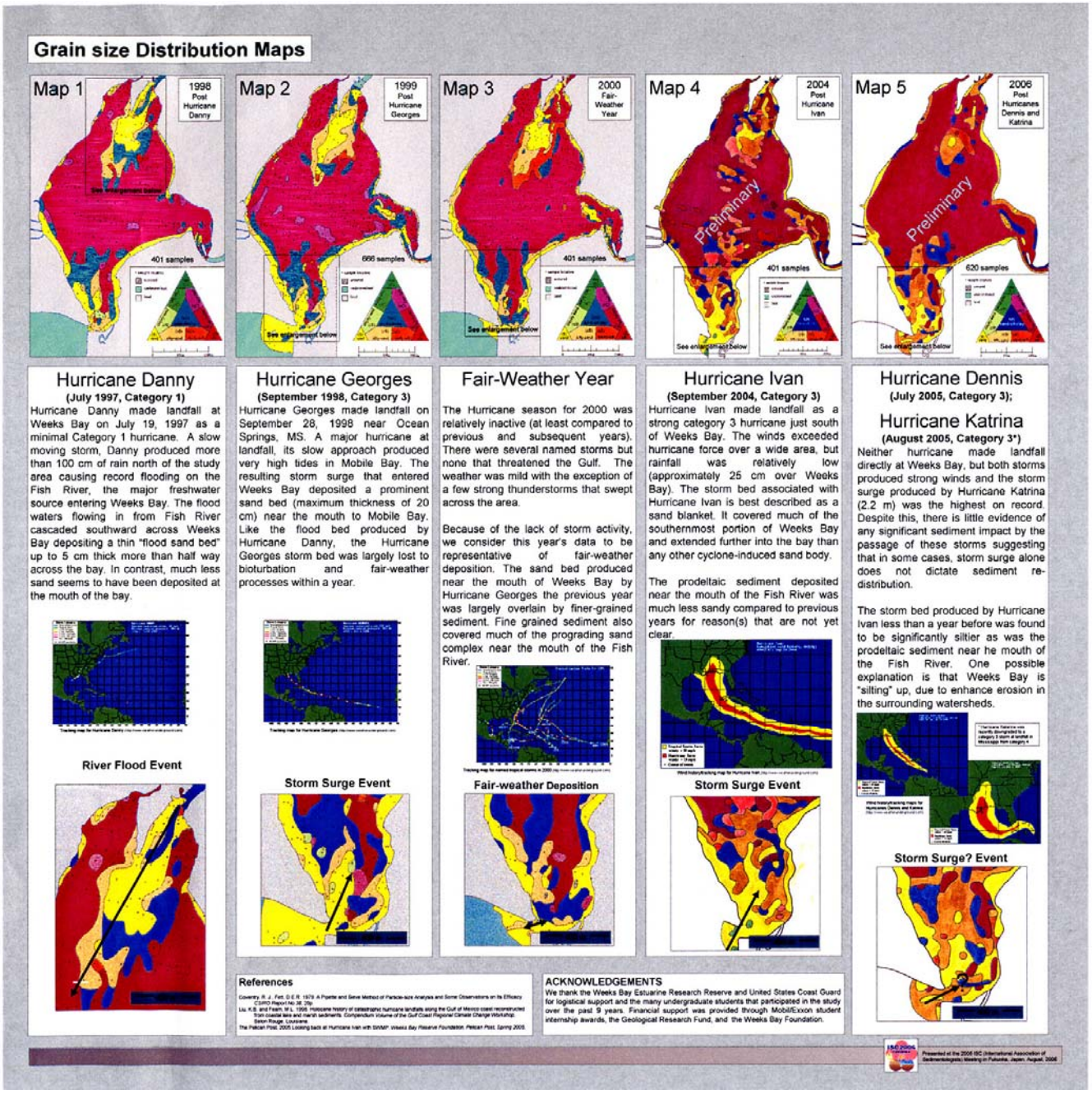

圖三、第 17 屆沉積大會壁報論文之一

The Effects Of Multiple Hurricane Impacts On A Small Gulf Coast Estuary, Weeks Bay, Alabama, USA

DOUGLAS W. HAYWICK, MEGHAN L. BRENNER, PETRA WEBB

Department of Earth Sciences, University of South Alabama, Mobile, AL USA 36688

Summary

This poster summarizes the results of nine years of bottom sediment monitoring in a small Northern United States Gulf Coast estuary. During this period, Weeks Bay (Figures 1, 4, 6) has been directly impacted by five cyclones. Fortunately for us, the wind patterns, storm surges, rain fall and storm duration of each of these events was highly variable permitting us to draw conclusions about the sedimentary impact of tropical storms on estuarine depositional environments.

Hurricane Danny (July, 1997) was a Category 1 hurricane on the Saffir-Simpson scale that stalled directly over Weeks Bay for two days. The storm was considered more of a "rain maker" than a "wind generator and the resulting flood surge that poured into the bay from the Fish River generated a sandy "flood bed" (cf. storm bed) that was deposited nearly half way across the bay (Map 1). The sand bed was lost via bioturbation within a year.

Hurricane Georges (September, 1998) was a Category 3 storm that made landfall well to the west of the study area, but onshore winds pushed an appreciable storm surge into Weeks Bay that deposited a sand bed several hundred metres into the estuary (Map 2).

Hurricane Ivan (September, 2004) was also a Category 3 storm, but it made landfall just to the south of the study area. The eye passed directly over Weeks Bay within a few hours of landfall (Figures 3, 5). This cyclone produced the greatest sedimentological change of any event within the study period. The sand bed that was generated by the 1.7 m storm surge extended well into Weeks Bay (cf. Map 3- fair-weather year with Map 4– Hurricane Ivan).

Hurricanes Dennis and Katrina made landfall to either side of Weeks Bay in, respectively, July and August, 2005. The combined sedimentological effects of these cyclones (Map 5) were modest compared to earlier events like Ivan and Georges despite the fact that the storm surge of 2.2 m produced by Hurricane Katrina was the greatest on record for Weeks Bay (S. Phipps, 2006, pers.comm).

Figure 1: Oblique aerial photograph of Weeks Bay looking to the north from 300 m above Mobile Bay.

Introduction

Residents of the United States Gulf Coast experienced several intense tropical storms in 2004/5 and some (e.g., Hurricanes Ivan, Dennis and Katrina), devastated portions of the shoreline (Figure 2). Media attention and pubic awareness generally focused on the human impacts of these hurricanes, but the role of tropical storms in coastal sedimentation was essentially ignored. That storms and fair-weather processes both affect coastal sedimentation has been satisfactorily demonstrated in previous studies (e.g., Liu and Fearn, 1998), but apart from knowing that sand washed away from a beach must end up somewhere else, the public (and many coastal managers) are ignorant about more subtle changes in estuarine sediment distribution.

Figure 2: Collapsed condominiums along Orange Beach, AL following the landfall of Hurricane Ivan.

Over a nine year period, undergraduate students in the Department of Earth Sciences have monitored bottom sediment distribution in Weeks Bay, a small (c. 7 km²) brackish embayment adjacent to Mobile Bay in south-western Alabama. Weeks Bay has proven to be an excellent sedimentology study site for three reasons: (1) the small size of the bay limits the scope of the work to manageable levels suitable for undergraduate students; (2) it is close to the University of South Alabama limiting travel and research-related expenses and most importantly; (3) the bay has been impacted by five hurricanes over the nine year time frame of the study (Danny, 1997; Georges, 1998; Ivan, 2004; Dennis, 2005 and Katrina, 2005).

The purpose of this study was to assess the impact of multiple hurricanes on the bottom sediment of Weeks Bay. This poster summarizes these data in a series of bottom sediment grain size distribution maps. Weeks Bay was sampled in January 1998, January 1999, January 2000, December 2004 and February-March 2006. .

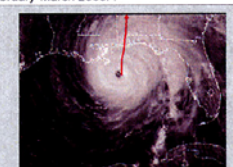

Figure 3: Satellite image of Hurricane Ivan several hours before landfall just south of Weeks Bay. The path of the storm is indicated by the red line.

The Study Area

Weeks Bay (Figures 1, 6) is a typical estuarine environment for this part of the northern Gulf Coastal Plain. It is shallow (generally less than 1 m deep), and is fringed by marshes, swamps and coastal forests. The bay is mostly floored in fine-grained, partially anaerobic sediment that hosts a significant benthic population of crabs and shell fish. Bioturbation down to several cm is pervasive over much of the central bay. Two main streams drain into Weeks Bay; Fish River (in the north) a and the Magnolia River in the east (Figure 1). There is a single inlet to Mobile Bay located in the southern-most portion of the bay. The inlet is tidally-dominated; however, the Alabama Gulf Coast is microtidal and experiences diurnal tides of less than 0.5 m. Tides within Weeks Bay are similar based upon data recorded by two water level gauges located in the northern and southern portions of the estuary.

Figure 4: Generalized location map of Weeks Bay in southwestern Alabama, USA.

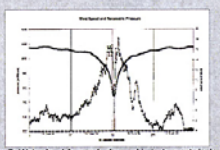

Figure 5: Water level from a hydrographic instrument deployed near the mouth of Fish River during passage of Hurricane Ivan in September 2004 (The Pelican Post, 2005).

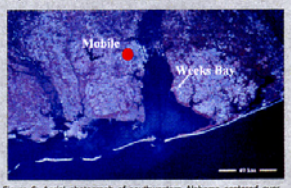

Figure 6: Aerial photograph of southwestern Alabama centered over Mobile Bay and the city of Mobile, AL. NASA Landsat image.

Methods

Bottom samples were collected using a Ponar grab sampler from a small boat (Figure 7). We were careful to only collect the upper 1 to 2 cm of sediment ("surface sediment"). The location of each sampling station (+/- 5-10 m) was determined with a WAAS-enabled GPS. Samples were transported back to the Sedimentology Laboratory at the University of South Alabama in preparation for grain size analysis.

Figure 7: Grab sampling bottom samples from Weeks Bay

Each sample was allowed to dry under a fan until completely dehydrated (usually 2-4 days). A 6 to 15g fraction of each sample was weighed and then transferred into a shaker container into which 150 ml of distilled water and 10 ml of a 10% solution of sodium hexametaphosphate had been placed. The samples were allowed to soak overnight in order to break apart the clay minerals as much as possible. The following day, the samples were disaggregated on a shaker table before being transferred to 1000 ml hydrological cylinders (Figures 8, 9).

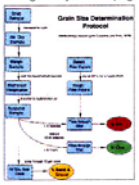

Figure 8: Flow chart illustrating the pipette and sieve method of grain size analysis used in this study (based upon Coventry and Fett, 1979)

We employed the Pipette and Sieve method of grain size analysis (Coventry and Fett, 1979) using 47 mm diameter glass fibre filter (pore diameter 0.5 microns) to collect 10 ml aliquots of silt and clay suspensions. The >63 micron fraction was determined through sieving after initially passing the remaining 980 ml sediment suspension of each sample through a 63 micron wet sieve.

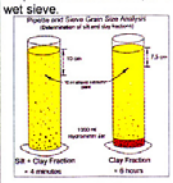

Figure 9: Schematic of a hydrological cylinder used for grain size analysis indicating approximate extraction depths and times to determine %silt + clay and % clay.

Grain size distribution maps for 2005 (Map 4) and 2006 (Map 5) are preliminary at this point in the study. Once the data have been confirmed, the 2005/2006 maps will be digitized using CorelDraw v 11 and/or AutoCAD and MapCAD software.

圖四、第 17 屆沉積大會壁報論文之二

P-094 Chemical composition and Ichnofacies of mudstones of the Lower Triassic Osawa Formation in the Ogatsu area, South Kitakami Terrane, northeast Japan

AKIKO YAMANAKA and KOHKI YOSHIDA
Geological Department, Faculty of Science, Shinshu University

1. The Objective of Research

The Early Triassic period is considered to be an interval of delayed biotic recovery following the end-Permian mass extinction. An analysis of the lower Triassic marine sediments suggests that severe environmental stress produced by peculiar marine conditions suppressed the Early Triassic recovery in the ecological and biological realms (Wignall et. al.,1998 ; Twitchett, 1999 ; Payne et. al., 2004). This study aims at reconstructing the Early Triassic shelf environments recorded in the mudstones of the Lower Triassic strata (Spathian) in Japan.

2. Methodology

A sedimentary facies analysis was carried out for the Inai Group in the Ogatsu and Motoyoshi areas, prior to laboratory work. Additionally, all of the samples for ichnological study and for geochemical study were collected from the Osawa Formation (Spathian). Ichnofabric indexes which represent the frequency of bioturbation was estimated under the microscope, and was divided into five levels based on Bottjer and Droser (1994). The diameters of trace fossil burrows are also estimated. The chemical compositions of the major and trace elements were measured using XRF. U, Th and rare earth elements were measured using ICP-MS.

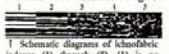

↑ Schematic diagrams of Ichnofabric indexes (1) through (5). (1) is no bioturbation recoded. (5) is completely

Terrigenous elements	→ Al, Ti, Si, Zr, Th, REE
Biological elements	→ Ca, Mn, P, Sr
Authigenic elements	→ Ce^{4+}(in Otic condition) U(in Reductive condition)

↑ The origin of the elements in sedimentary rocks.

3. Geological setting

The Triassic Inai Group is divided into four formations. This group unconformably overlies the upper Permian Toyoma Formation. Fossil *Ichthyosaurus* was reported ubiquitously in the Osawa Formation (Shikama et al.,1978 and Minoura et al., 1993).

In the Ogatsu area, the Osawa Formation is divided into the lower and upper members based on the lithofacies. The lower member of the Osawa Formation (LM) mainly consists of relatively massive, intensely bioturbated calcareous siltstones. Numerous burrows in cm-order are observed in the LM. The upper member of the Osawa Formation (UM) comprises parallel laminated mudstones with turbidite sandstones.

In the Motoyoshi area, the Osawa Formation mainly comprises parallel laminated mudstones with turbidite sandstones.

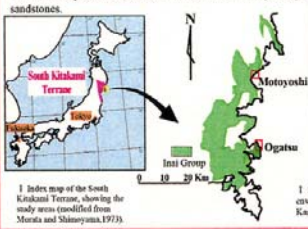

↑ Index map of the South Kitakami Terrane, showing the study areas (modified from Murata and Shimoyama,1973).

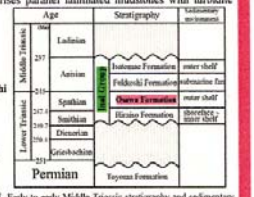

↑ Early to early Middle Triassic stratigraphy and sedimentary environment of the South Kitakami Terrane (compiled from Kamada and Takizawa, 1992 and Ehiro, 2002).

4. Ogatsu area

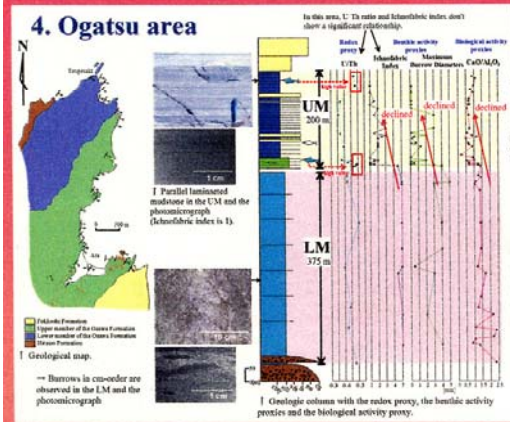

↑ Geological map.

→ Burrows in cm-order are observed in the LM and the photomicrograph

↑ Parallel laminated mudstone in the UM and the photomicrograph (Ichnofabric index is 1).

↑ Geologic column with the redox proxy, the benthic activity proxies and the biological activity proxy.

← Analyses using The X-ray Analytical Microscope. The compositional range of Fe (probably Pyrite) is shown by red. Pyrite formed around the lamina.

↑ Framboidal Pyrite in the clay lamina. This is a same horizon observed HCS and containing the fragment of fossil *Ichthyosaurus*.

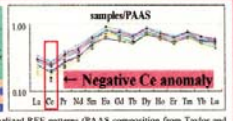

↑ PAAS normalized REE patterns (PAAS composition from Taylor and McLennan,1985). Negative Ce anomaly represents that they were deposited under the reductive condition.

↑ HCS represents that they had been deposited at a transitional zone between an inner and an outer shelf. And they also contain the fragment of fossil *Ichthyosaurus*.

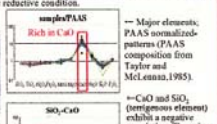

← Major elements; PAAS normalized-patterns (PAAS composition from Taylor and McLennan,1985).

←CaO and SiO_2 (terrigenous element) exhibit a negative correlation. The values of CaO should be reflected by the quantity of shelled organisms composed

↑ Low diversity: Photomicrograph showing low diversity of Trace fossils (*Phycosiphon*, *Planolites* and only minor *Chondrites*).

★The benthic activity in the LM is more intensive than those in the UM. The horizon showing HCS and containing the fossil *Ichthyosaurus* also includes the framboidal pyrite. Chemical redox proxies also suggest ireductive condition.

5. Motoyoshi area

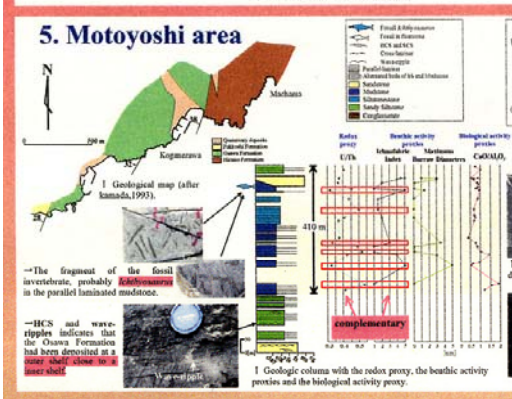

↑ Geological map (after Kamada,1993).

→The fragment of the fossil invertebrate, probably *Ichthyosaurus* in the parallel laminated mudstone.

→HCS and wave-ripples indicates that the Osawa Formation had been deposited at a outer shelf close to a inner shelf.

↑ Geologic column with the redox proxy, the benthic activity proxies and the biological activity proxy.

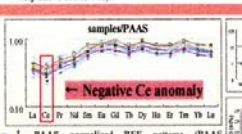

↑ PAAS normalized REE patterns (PAAS composition from Taylor and McLennan,1985). Negative Ce anomaly represents that they deposited under the reductive condition.

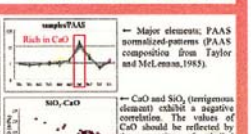

← Major elements; PAAS normalized-patterns (PAAS composition from Taylor and McLennan,1985).

←CaO and SiO_2 (terrigenous element) exhibit a negative correlation. The values of CaO should be reflected by the quantity of shelled organisms composed of $CaCO_3$.

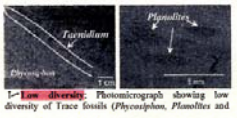

↑ Low diversity: Photomicrograph showing low diversity of Trace fossils (*Phycosiphon*, *Planolites* and

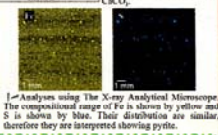

↑ Analyses using The X-ray Analytical Microscope. The compositional range of Fe is shown by yellow and S is shown by blue. Their distribution are similar, therefore they are interpreted showing pyrite.

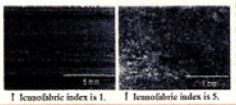

↑ Icnnofabric index is 1. ↑ Icnnofabric index is 5.

★ Many intervals are characterized by the deposits in reductive condition, rare or lacking benthic activity is intercalated. Furthermore, a part of them include the fossil vertebrates, probably

Respective features

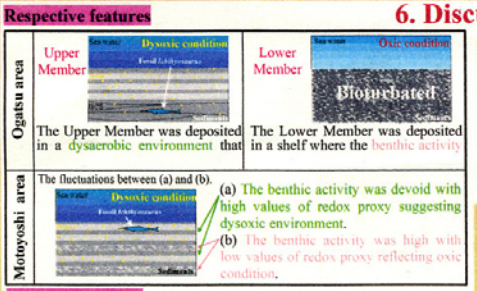

The Upper Member was deposited in a dysaerobic environment that

The Lower Member was deposited in a shelf where the benthic activity

The fluctuations between (a) and (b).

(a) The benthic activity was devoid with high values of redox proxy suggesting dysoxic environment.

(b) The benthic activity was high with low values of redox proxy reflecting oxic condition.

Common features

It seems like that the negative Ce anomaly and the low diversity of ichnospecies indicate the Spathian mudstone was influenced by dysoxic water column .

In the two study areas, they record similar oceanic event e.g. occurring **the dysaerobic environment in a shelf** during the early Triassic period (Spathian).

6. Discussion

The Osawa Formation in the South Kitakami Terrane is characterized by ubiquitous parallel laminated mudstones (Murata and Shimoyama, 1973). Therefore, the possibility of extended period of dysaerobic shelf conditions in the South Kitakami Terrane during the Early Triassic is suggested. The cause is estimated such hypothesis as follows.

·The increased productivity caused a local anoxic condition.
·The ventilation was stopped by the existence of closed sedimentary basin.
·They could probably compare the nature with Early Triassic anoxic event (e.g. Wignall and Hallam, 1992).

7. Conclusion

(1) Based on the lithofacies, the Osawa Formation had been deposited in a transitional zone between an inner and an outer shelf.
(2) Based on the ichnofacies and the chemical proxies, there was fluctuation between the oxic and dysoxic conditions (despite the fact that they were deposited in a shelf environment) during the Spathian Osawa Formation deposited. And dysoxic environment preserved the fossil *Ichthyosaurus* without the trace fossils. Furthermore the negative Ce anomaly represents the Osawa Formation deposited under relatively low oxic environment.

☆e-mail: s06a408@shinsyu-u.ac.jp

圖五、第 17 屆沉積大會壁報論文之三

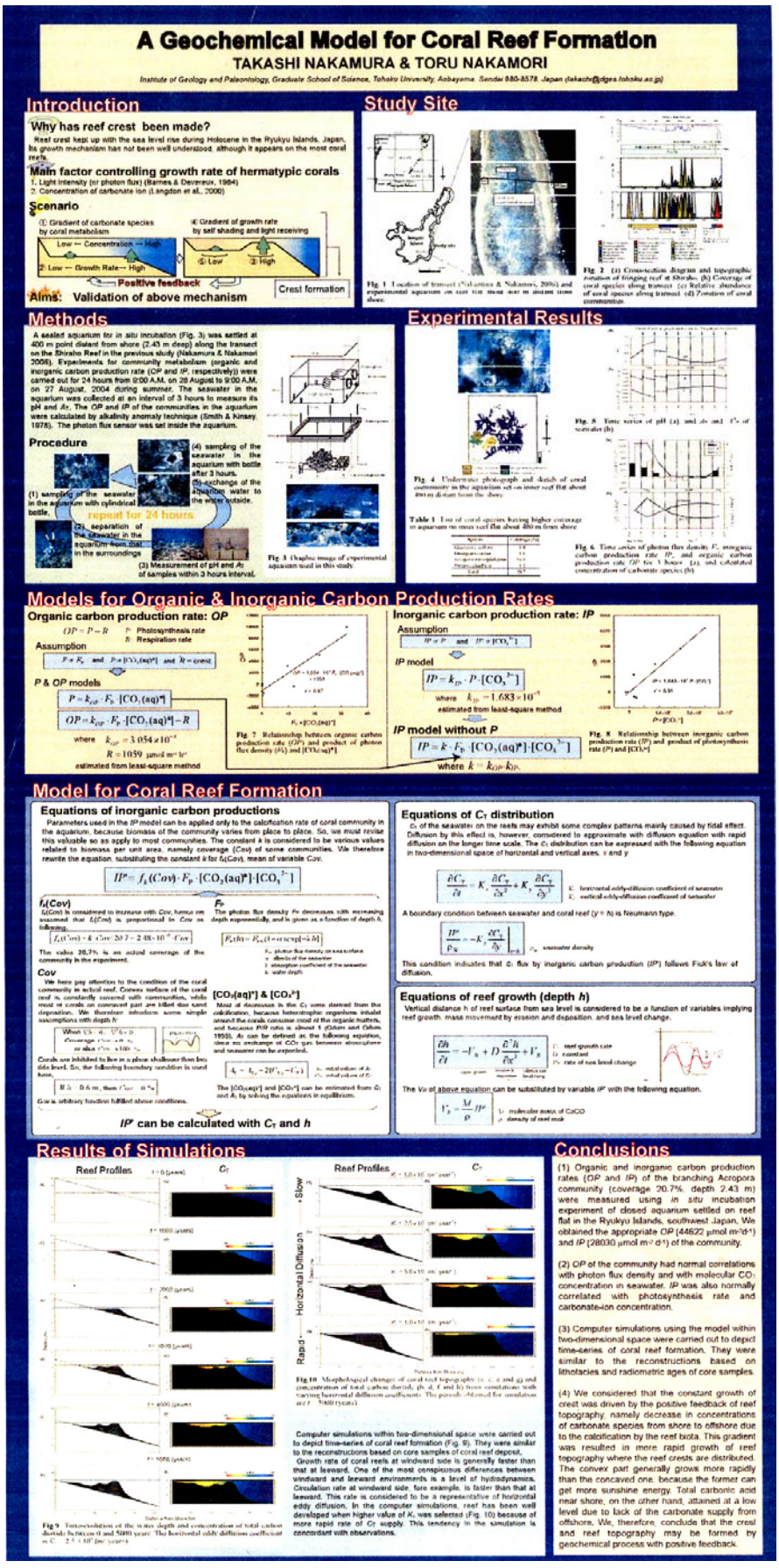

圖六、第 17 屆沉積大會壁報論文之四

Sedimentary Facies and Formation of Atoll Islands in the Pacific

Toru Yasukochi[1], Hajime Kayanne[1], Toru Yamaguchi[2] and Hiroya Yamano[3,4]

1: Earth & Planetary Science, the University of Tokyo, 2: Ethnology and Archaeology, Keio University, 3: National Institute for Environmental Studies, 4: Institut de Recherche pour le Development

1. Introduction

Reef islands on atolls are small and low-lying, composed largely of unconsolidated Holocene calcareous sand and gravel. Thus they are highly vulnerable to the impacts of sea-level rise as is anticipated as a result of the greenhouse effect. Approximately 500 atolls are distributed worldwide, and most of the atolls exist in the Pacific Ocean. Understanding how these islands were formed in the past will provide insights to prediction of there response to anticipated sea-level rise.

Several studies have been performed on reef-island morphology, but sedimentological studies have not been carried out on the Pacific atolls.

In this study, we excavated some trenches on Laura Island, Majuro atoll, in order to research its sedimentary facies and reconstruct the island formation.

2. Locality

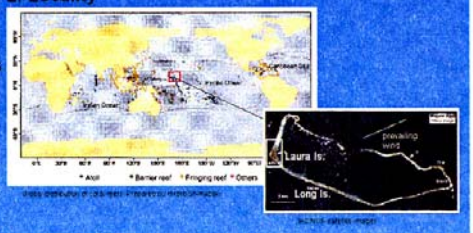

3. Sedimentary facies of Laura Island

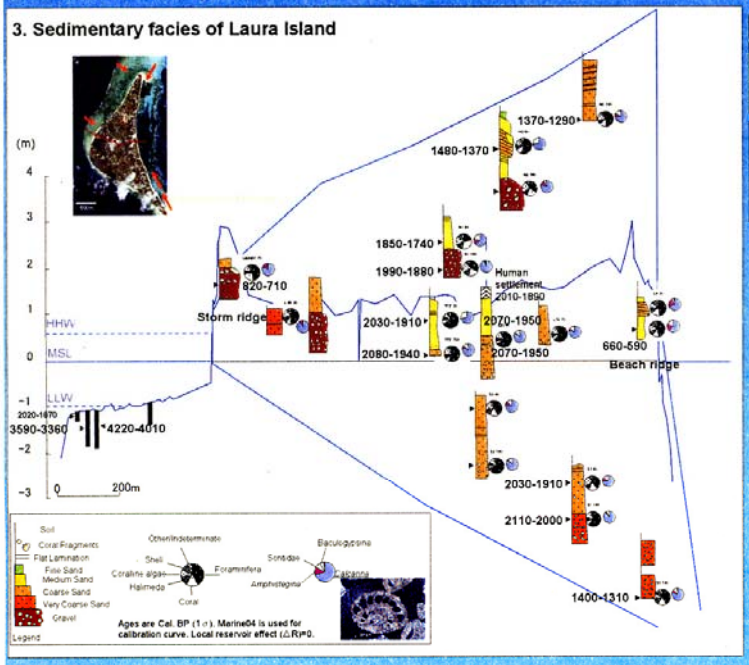

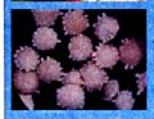

2 x 1 m trenches were excavated to depth of ca. 2 m on Laura Island, Majuro atoll.

Radiocarbon ages were obtained from tests of *Calcarina* that still had some spicules, according to the idea that these foraminifera had lived just before the sedimentation (Yamano *et al.*, 2001). ^{14}C age was measured in Geo-Science Lab.

Obtained ^{14}C ages were corrected for isotopic fraction and corrected to Cal. BP by Calib510.

Calibrated ages were around 2000 yBP at both the lower and the upper parts of the central sedimentary body of the island, indicating that the formation of the central axis of the island was within approximately a hundred years. The lower horizon consists of coarse sand with gravels, and the upper horizon consists mainly of well-sorted medium to coarse sand.

Larger benthic foraminifera are the most abundant component in many sand layers.

Calcarina, which lives on reef flat is the main component of foraminifera, indicating the sand was originally supplied from reef flat surrounding the ocean side of Majuro atoll. Considering the prevailing wind direction, the sand was probably transported mainly from northern reef and southern coast along Long Island.

4. Facies analysis

Gravels are considered to have been transported by relatively strong wave energy.

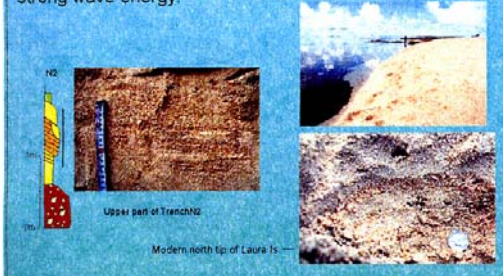

Sands are considered to have been transported by relatively calm wave energy. Assemblage of *Calcarina* tests forms parallel lamination.

5. Sea-level changes

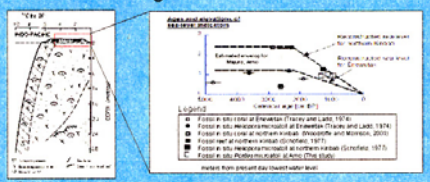

Coral reef grew up to the sea level which was >1m higher than modern sea level by ca. 4000yBP.

Sea level started falling about 2000yBP, which should changed ecological and physical environment of the reef flat.

6. Conclusion

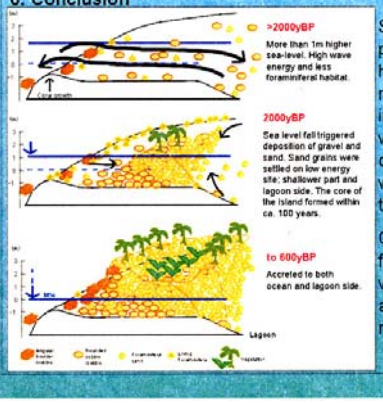

Sea-level fall around 2000yBP probably enlarged foraminiferal habitat, and made sediment on the reef flat more stable because impingement of wave became weaker (Scoffin, 1993), and/or diffraction of wave became stronger, which resulted in the formation of the reef island.

Quantitative evaluation of foraminiferal sand production and wave energy on the reef flat as against deposition of grains remains to be demonstrated.

圖七、第 17 屆沉積大會壁報論文之五

Three-Dimensional Grain Fabric

Clustering for Recognizing Dominant Combinations of Orientations and Shapes of Grains

TS3-1, P-048

Atsushi YAMAJI
Division of Earth & Planetary Sciences,
Kyoto University, Japan
E-mail, yamaji@kueps.kyoto-u.ac.jp
http://www.kueps.kyoto-u.ac.jp/~yamaji/

Miwa YOKOKAWA
Faculty of Information Science & Technology,
Osaka Institute of Technology, Japan

We propose a statistical technique for 3D grain fabric, useful for the analysis of 3D data obtained by X-ray CT, etc.

Summary

- Not only the major-axis orientations but also the shapes of grains should be treated simultaneously for the analysis of 3D grain fabric.
- The joint frequency of shapes and orientations of grains is represented by a point in a 5D parameter space, if the shapes are approximated by ellipsoids. And, the space can be constituted so as the points in the space to have one-to-one correspondences with the combinations of shapes and orientations of grains.
- The joint frequency is recognized as the clusters in the parameter space. So, density based clustering, a statistical technique, in the 5D parameter space can identify the frequently occurring combinations.
- The technique succeeded in identifying the groups of grains having similar orientations and shapes from artificial data.

Why are not only the orientations but also the shapes of grains necessary for recognizing 3D fabric?

TS3-1 The term 'fabric' refers to the orientations and packing of grains. Studies concerning the latter usually describe the dominant major-axis orientations of grains. However, the information of the orientations is not separable from that of shapes of grains for 3D grain fabric, even if the shapes are simply approximated by ellipsoids. On one hand, an oblate ellipsoid has no definite major-axis but its minor-axis orientation is significant for describing the attitude of the ellipsoid (Fig. 1). On the other hand, major-axis is significant for a prolate ellipsoid. Ellipsoids have a spectrum between them. The orientations of elongated or platy grains are more significant than those of spherical ones. The orientations of grains cannot be treated separately to investigate 3D grain fabric.

Accordingly, we propose a statistical method for recognizing the dominant combinations shapes and orientations of grains, the shapes of which are approximated by ellipsoids.

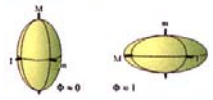

Figure 1. Oblate and prolate ellipsoids and their principal axes. M, I and m indicate the major-, intermediate- and minor-axes, respectively.

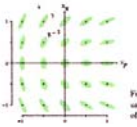

Figure 2. Elliott plot for indicating the shapes and orientations of ellipses.

Custering

One strategy to recognize 3D grain fabric is to use the cluster analysis of points in a parameter space, a point in which represent the specific combination of shape and orientation of an ellipsoidal grain. To make sense of the strategy, the points in the space should have one-to-one correspondences with the combinations.

Such a parameter space can be composed for 2D grain fabric: the Elliott plot of the shapes and orientations of elliptical grains exhibits the 2D parameter space for the data. One method for 3D grain fabric is an extension of the statistical method for studying 2D grain fabric that recognize the joint frequency of the shapes and orientations of elliptical grains. The joint frequency refers to the abundance of the combinations of shapes and orientations. Elliott (1970) used a 2D plot, on which a point represent the paired information, i.e., shapes and orientations (Fig. 2). The shape and orientation of an ellipse is indicated by the aspect ratio, R, and the major axis orientation, Θ. The ellipse is represented by a point on the Elliott plot, where the horizontal and vertical coordinates have the expressions,

$$x_E = (\log_e R)\cos 2\Theta \quad (1)$$

$$y_E = (\log_e R)\sin 2\Theta. \quad (2)$$

The origin of the plot represents circular grains, and points distant from the origin indicate elongated ones. Given a number of data, the joint frequency is shown by the density of points on the Elliott plot of the data (Figs. 2 and 3D). Hence, there is a powerful means of recognizing the joint frequency for the data, i.e., the cluster analysis or clustering of the points (Yamaji and Masuda, 2005).

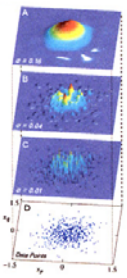

Figure 3. Three-dimensional plots of $D(\mathbf{x})$ with different scale sizes for the two-dimensional fabric data, the data points of which are depicted by the Elliott plot. Neighboring peaks coalesce into a smaller number of peaks by the increasing size σ.

Density base clustering

Tens of clustering methods have been proposed. We use density-base clustering, as the technique does not need to assume the number of clusters *a priori* (Tan et al., 2006). The density of points on the plot is evaluated by the continuous function of the position vector $\mathbf{x}$ on the plot (Fig. 3),

$$D(\mathbf{x}) = D(\mathbf{x},1) + \cdots + D(\mathbf{x},N),$$

where N is the number of grains, and

$$D(\mathbf{x},i) = \exp\left[-\frac{|\mathbf{x}-\mathbf{x}^{(i)}|^2}{2\sigma^2}\right]$$

indicates the contribution of the ith point to the density, and σ is termed the scale size. $D(\mathbf{x},i)$ represents a blurred image of the point: increasing value of σ makes the image more spread. The extremals of $D(\mathbf{x})$ indicate the dominant combinations of shapes and orientations. Fig. 3B shows two prominent peaks.

The scale size σ is the key of recognizing statistically significant clusters. Figs. 3A–C shows the peaks of $D(\mathbf{x})$ with different values of σ. When the value is much smaller than the representative distance between points, peaks appear at every data point. Increasing σ value amalgamates neighboring peaks, and all them eventually are united for large σ values. Statistically significant clusters are recognized as long-standing peaks for a variation of σ (Hinneburg and Keim, 1998; Nakamura and Kobtarnavar, 1998).

5D parameter space for 3D grain fabric

The Elliott plot works as the parameter space for 2D grain fabric: the combination of shape and orientation of an elliptical grain has a one-to-one correspondence with a point on the 2D space (Fig. 2). The space is two-dimensional, because the combination has two degrees of freedom, i.e., R and Θ. In addition, grains with similar combinations are mapped onto neighboring points on the plot, and vice versa.

Regarding 3D grain fabric, we need a higher dimensional parameter space: the shape and orientation of an ellipsoidal grain has 5 degrees of freedom. Specifically, the shape is denoted by the two non-dimensional parameters,

$$\text{aspect ratio} \quad R = a_2/a_3$$

$$\text{shape factor} \quad \Phi = (a_2 - a_3)/(a_1 - a_3),$$

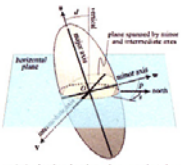

Figure 4. Angles denoting the major-axes orientations of an ellipsoidal grain. s and d are the strike and dip of the spanned by the intermediate- and minor-axes, and p is the pitch of the latter axis. The unit vectors, $\mathbf{u}$, $\mathbf{v}$ and $\mathbf{w}$, indicate the orientations.

where a_1, a_2 and a_3 are major-, intermediate- and minor-axis. Φ indicates the spectrum between prolate ($\Phi = 0$) and oblate ($\Phi = 1$) ellipsoids (Fig. 1). The attitude of an ellipsoid is indicated by three angles, e.g., the strike (s) and dip (d) of the plane spanned by the intermediate- and minor-axes and the pitch (p) of the latter axis (Fig. 4). Consequently, the five parameters (R, Φ, s, d, p) are needed for designating a combination.

Unfortunately, the 5D parameter space spanned by the axes of the Cartesian coordinates, O-$R\Phi sdp$, is not appropriate for our purpose, because a point in the space does not have a one-to-one correspondence to the combination. For example, this system cannot describe the attitudes of oblate ellipsoids, as they have indistinguishable major- and intermediate axes. Nearly prolate ellipsoids ($\Phi \approx 1$) can resemble to each other in their shapes and orientations, even if they have completely different p values (Fig. 4). We need an elaborate 5D parameter space, a point in which should have a one-to-one correspondence with the combination of shape and orientation of an ellipsoid.

For this purpose, we adapt the 5D parameter space of Sato and Yamaji (2006) to 3D fabric analysis. The space was originally defined for the statistical processing of stress ellipsoids. Design of a parameter space is critical to our problem, but it is somewhat complicated. So, the details of the parameter space are given in Appendix A.

As a result, the set of 5D position vectors, $\mathbf{x}^{(1)}, \ldots, \mathbf{x}^{(N)}$, represents the fabric data, which consists of the shapes and orientations of N grains. We search for the peaks of the function

$$F(\mathbf{x}) = \frac{\zeta_5}{N}\frac{R^2}{3}\sum_{i=1}^{N}|\mathbf{x}^{(i)}|^4 D(\mathbf{x},i)$$

instead of $D(\mathbf{x})$, where $\mathbf{x}$ is a 5D position vector, $(R\pi^2/3)|\mathbf{x}|^4$ is the surface area of the hypersphere with the radius of $|\mathbf{x}|$ and works as the correction factor of $D(\mathbf{x},i)$.

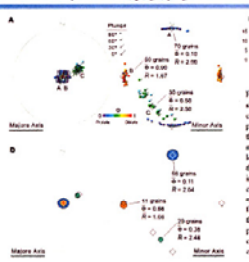

Figure 5. A) Paired stereograms (lower-hemisphere, equal-area projection) showing the principal orientations of the 150 ellipsoidal grains of the test data consisting of Groups A, B and C. A symbol like a tadpole indicates the principal orientations of a grain. Position of the head of the tadpole indicates the major-axis orientation in the left stereogram. Azimuth and plunge of the minor-axis orientation of the same grain are indicated by the direction and length of the tail, respectively. A shorter tail depicts a steeper minor-axis. In the right stereogram, the colors of head and tail are inverted. Shape factor, Φ, is indicated by a color bar. A diamond indicates the mean principal orientations of the grains belonging to a group. R and Φ are the mean aspect ratio and mean shape factor of grains. B, C) Histograms of aspect ratio R and shape factor Φ of the test data. D) Paired stereograms showing the detected groups through the present method with $\sigma = 0.15$ from the test data. Colors of circles plotted on the stereograms indicate the mean Φ of a detected group. Diameter of the circle shows the number of grains. Diamonds indicate the principal orientations assumed for Groups A, B and C.

Test

The present method was tested using an artificial dataset with known answer: the data included 150 ellipsoidal grains and were subdivided into three groups A, B and C. It was not possible to distinguish the groups by their principal orientations alone, because Groups A and B had approximately same major-axis orientations and the minor-axis orientations of Group C bridged the gap between those of Groups A and B (Fig. 5A). However, they have distinctive Φ values (Fig. 5C).

The data points corresponding to the ellipsoids made three distinctive clusters in the 5D parameter space (Fig. 6), therefore, they were easily identified by our method. Fig. 5D shows the satisfactory result. The three groups were recognized as long standing peaks for various σ values. The principal orientations and shapes corresponding to the centroid of the clusters in the parameter space were accurate. Since the cluster corresponding to Group C had the largest spread in the space, the representative shape and orientation of the grains that was recognized as the cluster had the largest inaccuracy ($\sim$10°). Consequently, our method was successful in recognizing the three dominant combinations of shapes and orientations in the artificial dataset.

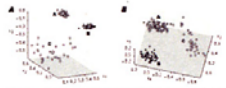

Figure 6. 3D plots showing the components of $\mathbf{x}^{(1)}, \ldots, \mathbf{x}^{(150)}$ for the test data (Fig. 6). Crosses indicate the centroids of clusters.

Appendix 5D parameter space

The mapping from the shape and orientation of an ellipsoid to a point in a 5D space is defined as follows. First, the orientation is denoted by the three unit vectors in Fig. 5: $\mathbf{u} = (u_1, u_2, u_3)^T$, $\mathbf{v} = (v_1, v_2, v_3)^T$ and $\mathbf{w} = (w_1, w_2, w_3)^T$. The orthogonal matrix

$$\mathbf{Q} = \begin{pmatrix} u_1 & v_1 & w_1 \\ u_2 & v_2 & w_2 \\ u_3 & v_3 & w_3 \end{pmatrix}$$

is defined using the components of the vectors. Second, the diagonal matrix

$$\mathbf{E}^* = \begin{pmatrix} 2-\Phi & 0 & 0 \\ 0 & 2\Phi-1 & 0 \\ 0 & 0 & -\Phi-1 \end{pmatrix}$$

is also constructed. Third, the symmetric matrix

$$\mathbf{E} = \frac{1}{A}\mathbf{Q}\mathbf{E}^*\mathbf{Q}^T \quad (3)$$

is calculated, where $A = \sqrt{3\Phi^2 - 3\Phi + 3}$. It can be shown that $\mathbf{E}$ has a one-to-one correspondence with the combination of the orientation and Φ (Yamaji and Sato, submitted). Fourth, we make the 5D vector,

$$\mathbf{x} = \begin{pmatrix} -\left(\frac{1}{3}+\frac{\Phi}{6}\right)E_{11} + \left(\frac{1}{3}-\frac{\Phi}{6}\right)E_{22} + \frac{1}{\sqrt{2}}E_{23} \\ \left(\frac{1}{3}-\frac{\Phi}{6}\right)E_{11} - \left(\frac{1}{3}+\frac{\Phi}{6}\right)E_{22} + \frac{1}{\sqrt{2}}E_{31} \\ E_{12} \\ E_{31} \\ E_{23} \end{pmatrix}$$

where E_{ij} is the ijth component of $\mathbf{E}$. Thanks to the factor 1/A in Eq. (3), $\mathbf{x}$ has a unit length. Finally, the position vector in a 5D space, $\mathbf{x} = (\log_e R)\mathbf{x}$, represents the shape and orientation of the ellipsoid. As a result, the 5D Euclidean space that accommodates this vector works as the parameter space, a point in with has a one-to-one correspondence with the combination of the shape and orientation of an ellipsoid in the physical space.

One a cluster center is identified at the end point of the position vector $\mathbf{x}$ in the 5D parameter space, the shape and orientation of the ellipsoid that is represented by the point are determined through the following procedure. First, the aspect ratio of the ellipsoid corresponding to the point is calculated as $R = \exp(|\mathbf{x}|)$, and we obtain the unit vector $\mathbf{e} = \mathbf{x}/|\mathbf{x}|$. This vector has a one-to-one correspondence to $\mathbf{E}$. Accordingly, $\mathbf{E}$ is obtained from this vector. Then, $\mathbf{u}$, $\mathbf{v}$ and $\mathbf{w}$ are obtained as the eigenvectors of $\mathbf{E}$, and Φ is calculated from the eigenvalues this matrix.

References

Elliott, D., 1970. Determination of finite strain and initial shape from deformed elliptical objects. *Geol. Soc. Am. Bull.*, **81**, 2221–2236.

Hinneburg, A., and Keim, D., 1998. An efficient approach to clustering in large multimedia databases with noise. In: *Proceedings, Fourth International Conference on Knowledge Discovery and Data Mining*. New York, AAAI Press, 58–65.

Nakamura, E., and Kobtarnavar, N., 1998. Determining number of clusters and prototype locations via multi-scale clustering. *Pat Recog. Let.*, **19**, 1265–1283.

Sato, K. and Yamaji, A., 2006. Embedding stress difference in a parameter space for stress tensor inversion. *J. Struct. Geol.*, **28**, 957–971.

Tan, P-N., Steinbach, M. and Kumar, V., 2006. *Introduction to Data Mining*. Pearson, Boston, 769p.

Yamaji, A. and Masuda, F., 2005. Improvements in graphical representation of fabric data, showing the influence of aspect ratios of grains on their orientations. *J. Sediment. Res.*, **75**, 517–522.

Yamaji, A. and Sato, K., submitted. Distances for the solutions of stress tensor inversion in relation to misfit angles that accompany the solutions. *Geophys. J. Int.*

Yokokawa, M., Iwata, H., Tenchiyama, A., Uemgi, K., Nakano, T., Endo, N. and Okazawa, T., 2004. Three dimensional analyses of texture of sandstone using X-ray microtomography. *SPring-8 User Expert Rep.*, **12**, 113.

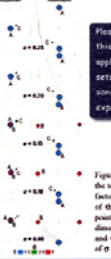

Please visit the poster by Nishio et al. in this session (TS3-1, P-049) for the applications of this technique to the data sets acquired by X-ray CT from the sands that were deposited in an experimental flume.

Figure 7. Results of the method applied to the test data with various scale sizes. Shape factor is indicated by colors. The diameter of the circles denotes the number of data points belonging to a cluster in the five-dimensional parameter space. Groups A, B and C were clearly separated for the case of $\sigma = 0.15$.

圖八、第 17 屆沉積大會壁報論文之六

照片一、壁報展示情形之一

照片二、發表論文會場之一

照片三、展覽會場之一

照片四、岩心分析展示

照片五、國際油公司參展之一

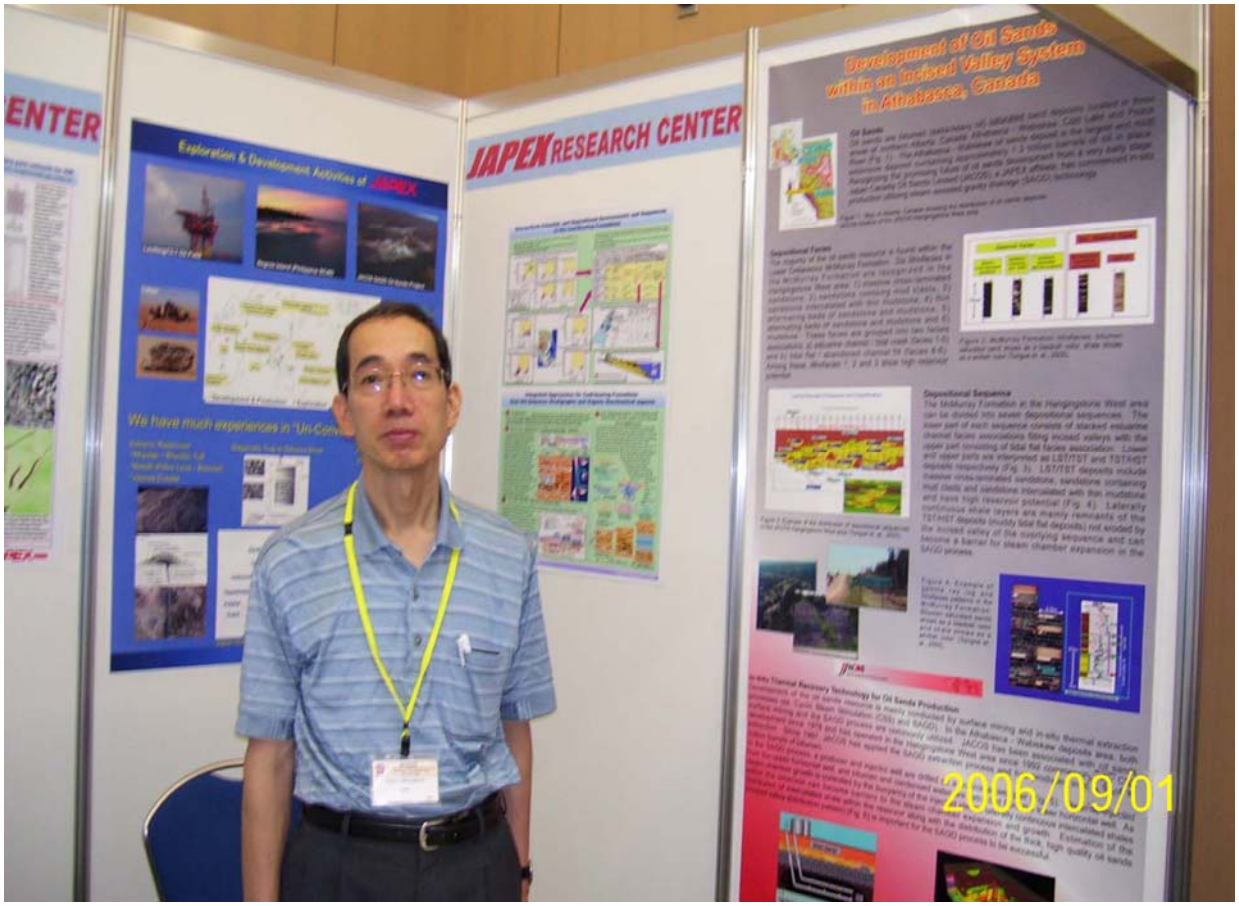

照片六、日本油公司參展之一

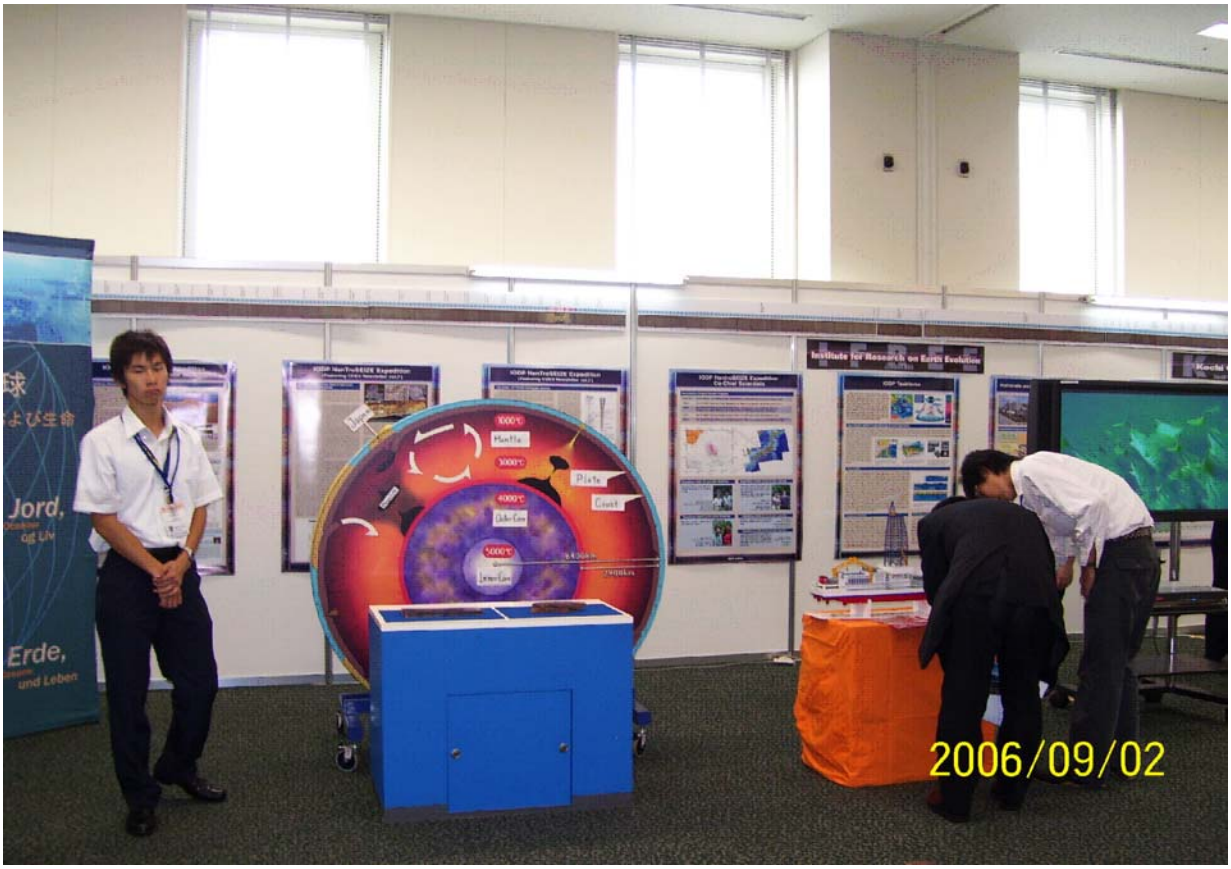

照片七、大學參展場景之一

照片八、發表會場外作者準備情況之一

照片九（a.b.）野外勘查之一

照片十（a.b.）野外勘查之二

照片十一（a.b.）野外勘查之三

照片十二（a.b.）野外勘查之四

四、研討心得

本次參與此國際研討會除一般有關古生物。沉積外，特別注意研討有關高分辨層序地層分析技術，有關研討心得如下：

一、研討建立高分辨層序地層架構分析技術

（一）震測層序架構

震測層序架構的研究是以震測反射資料為基礎的。震測反射界面基本上是等時面或平行於地層內的等時界面，而地層基準面旋迴與界面具有成因地層單元和時間界面的含義，因此震測反射界面平行於或相當於基準面旋迴的界面。

解釋有 7 個步驟：1. 震測層序分析；2. 測井層序分析；3. 用合成震波聯結並與生物地層結合；4. 震測相分析；5. 岩相與沉積環境的解釋；6. 震測模型正推或反推；7. 綜合解釋及繪圖。

1. 建立震測層序架構的基礎

首先在進行區域古地理和構造運動分析的基礎上，選擇好標準震測剖面。在探勘的地區，應在進行全面重力、磁力和震測資料綜合分析的基礎上，把現有的震測測線都進行詳細的震測層序分析，選擇一個標準剖面網，以便從不同方位追蹤判別震測層序，並選取其中較好張裂構造剖面，作為震測層序架構標準剖面。

2. 層序邊界及震測層序劃分

所謂震測層序就是從震測剖面識別出以不整合面及其與之可以對比的震測反射為界，內部反射相對一致的震測反射單元。劃分震測層序首先就是要識別限定震測層序的界面。按照層序定義，震測層序邊界為不整合及與之可以對比的整合面在震測剖面上的對應。而震測剖面上的反射波型特徵是地質事件的最好記錄。指示層序底界面的反射終止類型有上覆(onlap)和下覆

(Downlap)，指示層序頂界的反射型式有頂覆(Toplap)和截切(Truncation)。

3.碎屑岩和碳酸鹽岩沉積層序在震測剖面上的反射特徵及所代表的地質意義

在震測層序劃分的基礎上，通過研究層序內震測相的反射屬性便可進一步分析層序的沉積環境及古地理，重建盆地的沉積史和構造史。

不同構造背景下沉積的碎屑岩和碳酸鹽岩沉積層序，在震測反射剖面上的反射特性是不同的，並且同一沉積層序的不同體系域其反射特性亦不相同，並且都各自代表著不同的地質意義。

(二) 建立高分辨率井下層序地層架構

1.井下層序分析原則

井下層序分析主要依據測井資料和岩性地層解釋剖面。由於在工作中常常缺少系統岩心資料，因此，在層序分析時應特別注意：

(1)重點井的選擇。由於井所處的盆地位置的不同，在同一盆地不同地理位置的井所反映出的層序發育特徵是不同的。在研究中，盡量選擇位於凹陷深處地層發育齊全的深井來進行垂直方向層序分析，以建立各自凹陷中的垂向層序地層架構，通過測井曲線的深度一時間轉化合成記錄，進行測井一震測對比聯結。

(2)利用震測層序來訂定測井層序的級次。在垂向上，由於不同級次的層序不易區分，且由於它生旋迴與自生旋迴共存的干擾，不同人可能作出不同數目的層序。同時，由於一個反射層是由許多不同反射係數和不同阻抗的層面相互干涉所組成的，並且在用測井曲線進行對比解釋時往往存在某些不確定性和多解性。根據聲波曲線做成震測合成記錄，並與鄰近的實際震測資

料反複對比，以提高解析精度。同時，利用震測層序訂定測井層序中主要不整合面的位置來限定高級次的井下層序是至為重要的步驟。通過震測層序和沉積環境分析，確認各個時期鑽井所在的盆地古地理位置，從而可對各時期體系域發育特徵作觀察及瞭解，以減少在確定體系域性質上的失誤。由於震測與測井資料的解析度不同，將震測層序邊界標定到測井中，對應著井測曲線深度段其具體的邊界位置，需要對這一深度段的測井曲線作進一步分析，用這種方法可提高井下層序分析的可靠性。

(3)基準面上升到下降的轉換位置，即緻密段，是古生物發育、有機碳富集的層段，可以依據古生物種類、豐度、有機碳含量分析來幫助確定緻密段的位置，以及判定其從屬關係。

(4)多種資料綜合應用。層序劃分中盡可能利用岩性剖面、岩性分析和古生物資料進行綜合判斷，綜合分析各層序的形成條件和層序演化史。

2.確定短期基準面旋迴

(1)岩心短期基準旋迴

岩心短期基準旋迴的分辨：以岩心剖面來識別短期基準面旋迴，並以此來確定短期基準旋迴界面性質是非常重要的。利用岩心剖面的結構變化、地層終止方式和上下地層的接觸關係可以分辨出短期基準旋迴。在碎屑岩層序分析中的識別標幟有：

(A)河道沖刷侵蝕界面。該界面是由於基準面下降到地表之下時發生侵蝕作用而形成的界面，常發育河道塊狀砂岩和河底的滯留沉積物。

(B)作為層序界面的濱岸上覆相對於下伏地層向盆地方向遷移，表現為淺水相的粗粒沉積物直接覆蓋於深水的細粒沉積物之上。

(C)岩石類型或相組合的垂向剖面上轉換的位置，如水體向上變淺的相序或相組合向水體逐漸變深的相序或相組合的轉換處。

(D)砂、泥岩厚度旋迴性變化，如層序界面之下，砂岩粒度向上變粗，厚度向上變大，而泥岩向下變純、變厚。層序界面之上則相反。這種旋迴的變化特徵常以疊加模式的改變表現出來。

(E)反映水深、水體性質及沉積環境的泥岩原生顏色也可做為識別短期旋迴的依據。

(2)岩心短期基準面旋迴特徵

位於不同的沉積環境、處在不同相帶部位的岩心可以識別出不同相的微相類型，這些亞相或微相以特定的相序相組合構成了與短期基準面相當的短期地層旋迴。這種短期地層旋迴的厚度、對稱性都是不同 A/S 比值的響應，它們出現於特定 A/S 比值的中期基準面旋迴的特定位置上。需要提及的是，在同類可容空間控制下，由不同的相序組合成的短期旋迴，其岩性特徵、粒度、厚度、層理等可能並不相同。

(A)高可容空間的短期基準面旋迴：高可容空間的短期旋迴出現在中期基準面上升半旋迴至基準面下降半旋迴的轉換位置附近，此時 A/S 比值較高。

(B)低可容空間的短期旋迴：低可容空間的短期旋迴一般發育於最低可容空間，低 A/S 比值條件下的中期基準面旋迴的

兩個地層位置上，即中期旋迴的底部附近，或者基準面下降到上升的轉換點附近。

(C)中等可容空間的短期旋迴：此類短期旋迴主要發育於中等 A/S 比值條件下、中等可容空間旋迴中。中等可容納間的短期旋迴往往是不對稱或對稱性較差。基準面下降半旋迴發育的短期旋迴，往往出現在中期基準面上升半旋迴中。

中等可容空間的短期旋迴的相序或相組合與高可容納和低可容空間旋迴的相序或相組合特徵之間，呈現一種過渡的相組合或相序特徵，常表現在某種相序或相組合厚度的變化上。如在辮狀河砂岩沉積中，中期旋迴基準面下降半旋迴發育的中等可容空間的短期旋迴，其砂岩厚度大於高可容空間形成的短期旋迴的砂岩的厚度，而小於低可容空間的短期旋迴中的辮狀河砂岩的厚度。

(3)測井曲線的短期基準面旋迴

沉積岩是沉積物源及其搬運機理與沉積環境的產物，它可反映沉積物在經歷搬運、沉積和埋藏過程中的物理、化學條件的變化。其粒度、分選性及泥質含量與岩石的電阻率、天然放射性、自然電位都有良好的對應關系。由於這種岩石物理參數與沉積特徵的相關性，因此幅齒形曲線組合，實際上為正常淺湖相沉積，越岸沉積表現為中低幅一指形曲線組合。

3.測井曲線的中期基準面旋迴的確定及其特徵

(1).測井曲線中期基準面旋迴

具有特定疊加樣式的一組短期基準面旋迴組合構成中期基準面旋迴，它是在大致相似的地質背景下形成的一套成因上有聯系的岩石組合，這些疊加樣式常常具有鮮明的測井響應。向(湖)海盆方向推進的疊加樣式(進積)，形成於中期基準面下

降時期，此時 A/S<1，即沉積物補給速度大於可容空間增加速率。相鄰的短期旋迴，其上覆的短期旋迴在沉積學、岩石學方面的性質與下伏旋迴相比具有可容空間減小的特徵;向陸推進的疊加樣式(退積)形成於中期旋迴的上升時期，此時 A/S>1，即可容空間增加速率大於沉積物供給速率,上覆短期旋迴性質與相鄰下伏短期旋迴相比，在沉積學、岩石學方面表現為可容空間增大的特徵。短期基準面旋迴呈加積的疊加樣式，則出現在中期基準面上升到下降的轉換時期，A/S：1，相鄰短期旋迴形成時，可容空間的變化不大。利用以上三種短期旋迴的疊加樣式來確定中期旋迴。

(2)測井中期旋迴特徵

根據研究層段地層的岩性特點,選擇以自然伽馬測井曲線為主，電阻率與自然電位曲線為輔的測井系列劃分地層基準面。測井曲線基準面旋迴的確定，特別是層序界面性質的確定是在取心井段岩石一聲波特性標定的基礎上進行的。也就是說,首先要利用取心井建立短期旋迴的岩相組合與測井響應的對應模型，然後再運用到設取岩心之井中。

4.測井曲線的長期基準面旋迴

長期基準面旋迴反映了比中期基準面旋迴更長時間的基準面旋迴的變化,它是由若干個具有相同地質背景和沉積特徵的中期基準面旋迴相互疊加面形成的。長期基準面旋迴可與震測層序對比。

(三) 震測層序架構與井下層序架構對比

1.震測層序與鑽井下層序對比

震測層序和鑽井下層序是從兩個不同的途徑來分析盆地內層序地層架構。因此，利用合成震測記錄和/或測井深度一

時間轉換資料，將測井曲線標定到連井震測剖面中以檢驗震測和測井層序劃分的結果，最終完成盆地震測一井下對比方案，建立起盆地內綜合層序系統。其在陸相層序地層研究中尤為重要。此由於在陸相地層，尤其是在河流相地層中，許多沉積表現為近於平行的水平反射，震測層序及其界面的識別很難與大陸邊緣或海(湖)斜坡沉積中常用的不整合面或反映地層不協調的震測反射終止類型來分析。因而，震測地層的確定是通過合成記錄將自然電位與電阻率轉換成雙程傳播時間坐標，對連井震測剖面進行標定，並結合地層旋迴界面的震測標志和震測相的區域變化來進行。

2. 中、長期基準面旋迴相組合的平面作圖

在一個盆地中，盡管中長期旋迴內的相組合在平面上有較大的變化，但由於厚度、旋迴對稱性變化較小，因此可在盆地內進行追蹤與對比。同時由於高解析度二維和三維震測剖面可分辨的地層單元也可與鑽井、測井中可識別出的中長期旋迴相對應，而且震測相與幾何形態也可用中長期旋迴的性質加以解釋及預測，因此，中長期旋迴是一個地區高解析度地層架構建立與對比的基礎。在震測剖面上，對已確定的中長期旋迴進行封閉追蹤，並投影到平面圖上即可完成時間地層單元的平面作圖。

二、隨著層序地層學理論及其應用技術的不斷發展，其應用範圍已從早先單純的海相地層擴展到目前各種環境類型的地層，其研究精度已由原來的三級層序發展到高分辨率(四、五級)層序，並在油氣勘探和開發有著越來越重要的應用。隨著研究精度的提高，根据鑽、測井資料進行基準面旋迴劃分進而劃分層序的工作也變得更重要；同時，對同一口井、同一層段、同樣的資

料基礎，不同的人可能有不同的旋迴劃分結果，這也增加了旋迴識別劃分的不確定性。在電腦技術快速發展的今天，根据已有的基準面旋迴區別和劃分，可編制相應的電腦軟體，由計算機來進行基準面旋迴的識別與劃分，既節省了大量的工作量，又可以消除人為因素劃分的不確定性。

三、高分辨率層序地層分析技術至少可以在兩方面直接用於較精確的儲層描述和儲層預測研究，一是高分辨率的地層對比，由於控制流体流動路徑的絕大多數性質——岩石的岩性、物性、幾何形態和連續性，形成於沉積物在地貌環境中的沉積過程，因此，精確的地層對比可以揭示這些岩石性質的四維空間(時間—空間)的分布。二是高分辨率層序地層分析技術可以揭示對控制流体流動有重要作用的岩石性質和成因層序在較長期基準迴旋內所處地層位置之間的關系，與普遍認為沉積環境單獨控制地層特性的觀點不同，由於地層形成過程決定於沉積對應系統，沉積記錄的許多性質是沉積環境內可容納空間變化的函數。基準面旋迴變化伴隨著可容納空間的增加和減少，可容納空間控制了時間域內任何特定位置可能堆積的沉積物的最大量。從地層沉積過程(A／S 值變化)對儲集層控制作用之觀點出發研究儲集層，不僅可以提高儲集層特性的準確性和精確性，同時高分辨率時間地層對比還為把從鑽井獲取的一維信息轉變為三維地層關係預定量化，使地層幾何形態、大小和沉積相的位置、岩石物性的預測更加精確。

四、河相沖積地層的層序劃分一直是層序地層研究中的難處，主要是其基準面旋迴的識別比較困難，如一般很難分辨由河流改道等自旋迴作用形成的旋迴和與控制層序形成的其他旋迴作用產生的旋迴，或將基準面下降產生的河道切割不整合面與河道改道作用形成的不整合面加以區別。然而可應用層序地層方法

對沖積河流相進行分析。在河流相中基準面旋迴的判別方法有：

(一)較高級次的旋迴界面常是呈區域分布的規模較大的河道沖刷切割面。

(二)通過河道類型和河道砂体垂向組合的特征分析可容納空間的變化，進而劃分基準面旋迴。

(三)在河流相地層中“最大洪泛面”，即海(湖)相層序地層中的緻密段，處於基準面上升至基準面下降的轉換位置。在近海海岸平原河流相中該轉換位置較易判別，表現為海泛面的出現或受潮汐影響的河道沉積；在遠離海、湖盆位置的沖積平原中，基準面的上升常伴隨著地下水面的上升，在河間地區形成河間湖泊、湖沼或沼澤，具暗灰色泥岩、炭質泥岩、煤層或碳酸鹽岩發育為特徵。

五、在湖相沉積地層中，地層層序的劃分首先應判別地層記錄中的反映多級次基準面的地層旋迴。判別過程中應注意：

(一)鑽井主要基準面旋迴界面的確定

(二)最大湖泛面的識別

(三)震測強反射同相軸與層序界面

六、河湖沉積體係是陸相地層的重要組成部份，有許多主要的油氣資源均賦存其中。對湖相地層進行精準分析，可建立適合陸相地層的高分辨率層序地層模式及其研究方法，為該類沉積地層中的隱藏封閉預測及油藏精細描述提供理論基礎和模式指引。

五、結論與建議

多年來本所未派員參與有關國際沉積研討會，而從事盆地分析研究並協助現場單位探勘為本所之重點工作，在有關盆地地層架構、地層層序與對比、沉積環境分析、沉積相研究等課題是盆地探勘及石油系統的基礎，亦為礦區評估之首要工作。而此次參與第十七屆世界國際沉積大會，除一般有關古生物、沉積學外，特別注意研討有關高分辨層序地層架構建立與分析技術。

高分辨率層序地層分析技術至少可以在兩方面直接用於較精確的儲層描述和儲層預測研究，一是高分辨率的地層對比，由於控制流体流動路徑的絕大多數性質——岩石的岩性、物性、幾何形態和連續性，形成於沉積物在地貌環境中的沉積過程，因此，精確的地層對比可以揭示這些岩石性質的四維空間(時間－空間)的分布。二是高分辨率層序地層分析技術可以揭示對控制流体流動有重要作用的岩石性質和成因層序在較長期基準迴旋內所處地層位置之間的關系，與普遍認為沉積環境單獨控制地層特性的觀點不同，由於地層形成過程決定於沉積對應系統，沉積記錄的許多性質是沉積環境內可容納空間變化的函數。基準面旋迴變化伴隨著可容納空間的增加和減少，可容納空間控制了時間域內任何特定位置可能堆積的沉積物的最大量。從地層沉積過程(A／S 值變化)對儲集層控制作用之觀點出發研究儲集層，不僅可以提高儲集層特性的準確性和精確性，同時高分辨率時間地層對比還為把從鑽井獲取的一維信息轉變為三維地層關係預定量化，使地層幾何形態、大小和沉積相的位置、岩石物性的預測更加精確。

本次研討成果：

1. 可運用生物地層、沉積環境分析、沉積相及層序分析建立地層架構，做為盆地分析之基礎。

2. 收集新近國際地層對比資料建立研究礦區之對比。

3. 進行相關技術之交流。

4. 日後可應用於國內外礦區評估及探勘作業。

並建議公司：

（一）日後多派研究員參與相關研討以增進專業技術

（二）期研討會前後之訓練課程值得參與。

（三）藉助野外調查研討可收事半功倍之效。

（四）整合運用古生物、沉積學、地球物理、地球化學等專業在高分辨率層序地層分析工作。

（五）加強應用於盆地分析與國外探勘作業中。